Decision Feedback Detectors for SOQPSK

Erik Perrins and Balachandra Kumaraswamy
Department of Electrical Engineering & Computer Science
University of Kansas
Lawrence, KS 66045
E-mail: esp@ieee.org and balachk@ku.edu

***Abstract*— We consider highly-simplified decision feedback detectors for shaped-offset quadrature phase-shift keying (SOQPSK), a highly bandwidth-efficient and popular constant-envelope modulation. In particular, we show that the state complexity can be reduced to a minimal level—two states—with asymptotically optimum performance, as demonstrated by performance analysis and confirmed by computer simulations. The complexity reduction is achieved by a novel manipulation of the differential encoder and the SOQPSK *precoder*, which are both part of the transmission model for SOQPSK. We give two possible architectures for achieving this complexity reduction: the pulse amplitude modulation (PAM) technique and the pulse truncation (PT) technique. We also formulate these detectors for coherent and noncoherent detection. The resulting family of detectors makes use of recent advances in SOQPSK technology based on a continuous phase modulation (CPM) interpretation of SOQPSK. The proposed simplifications are significant since they *minimize* the complexity of trellis-based SOQPSK detectors, which have only become available in recent years. Since trellis-based SOQPSK detectors are 1–2 dB superior to the widely-deployed family of symbol-by-symbol SOQPSK detectors, the proposed two-state detectors offer the simplest means of achieving these performance gains. Thus, these simple detection schemes are applicable in settings where high performance and low complexity are needed to meet restrictions on power consumption and cost.**

I. Introduction

Shaped-offset quadrature phase-shift keying (SOQPSK) is a popular bandwidth-efficient special-case of continuous phase modulation (CPM) [1]. While CPM has a number of advantages, one advantage in particular is responsible for its widespread deployment: it has a constant signal envelope. This makes it compatible with nonlinear power amplifiers, which are highly efficient in converting limited (i.e. battery) power into radiated power. This in turn allows for a smaller (miniature) physical size and lower cost for the transmitter. To date, SOQPSK has been incorporated into military and aeronautical telemetry standards, although wider use is merited since it is applicable in any setting where bandwidth-efficient constant-envelope modulations are needed.

In addition to its name, SOQPSK shares a number of similarities with conventional OQPSK. These similarities are exploited at the receiver, where symbol-by-symbol OQPSK-type detectors are the most commonly deployed means of detecting SOQPSK, e.g. [2], [3]. The advantage of the OQPSK interpretation at the receiver is its *simplicity*. Thus, the *low-cost* advantage of SOQPSK can be shared by the transmitter and the receiver. However, the disadvantage of OQPSK-type detectors is that they ignore the *memory* that is inherent in the SOQPSK signal. Depending on the details of their construction, symbol-by-symbol OQPSK-type detectors are suboptimal by 1–2 dB when applied to SOQPSK [3]. This loss is significant since it erodes some of the power efficiency enjoyed by SOQPSK in the first place.

Because SOQPSK is a modulation with memory, its optimal detector requires a *trellis*. Such detectors were first studied only recently in [4], where a cross-correlated trellis-coded quadrature modulation (XTCQM) [5]–[7] viewpoint was taken for SOQPSK. The XTCQM model was applied to the simplest version, military standard SOQPSK, or "SOQPSK-MIL," and resulted in a detector with a four-state trellis. More recently in [8], a CPM interpretation of SOQPSK was applied at the receiver. This also resulted in an optimal four-state detector for SOQPSK-MIL; furthermore, the CPM-based approach opened the door for two reduced-complexity methods for detecting the more complicated version of SOQPSK adopted by the telemetry group, "SOQPSK-TG" [9]. These two techniques, pulse amplitude modulation (PAM) [10], [11] and pulse truncation (PT) [12], [13] result in four-state detectors for SOQPSK-TG that are within 0.2 dB of the impractical *512-state* optimum detector.

In this paper, we show that the size of the trellis can be reduced to its minimum—two states—for both SOQPSK-MIL and SOQPSK-TG. This is accomplished by a novel manipulation of the differential encoder and the SOQPSK *precoder* which leads to a simplified representation of the transmitter's state memory. This manipulation achieves for SOQPSK the same thing that minimal encoder representations achieve for convolutional codes, e.g. [14]. This simplified transmitter model, combined with decision-feedback at the receiver, yields the overall state reduction. We show how to implement this state reduction in a two-state detector using the PAM and PT techniques, in both *coherent* and *noncoherent* formulations. This results in a family of four distinct detectors, which demonstrates the versatility of the simplified state model.

For the coherent case, we use performance analysis to show that the two-state PAM and PT detectors have no losses relative to their four-state counterparts for asymptotically large signal-to-noise ratios (SNRs); however, the accompanying simulation results show that for moderate SNRs, the PT technique results in a negligible loss on the order of 0.1 dB.

The proposed reduction to two states is significant since the

major drawback of trellis-based detectors is their complexity compared to their symbol-by-symbol cousins. Since the proposed detectors reduce the state complexity to its minimum of two states, these detectors represent the most attractive means of realizing the 1–2 dB advantage trellis-based detectors have over symbol-by-symbol detectors.

The paper is organized as follows. In the next section we describe the signal model for SOQPSK, including the four-state transmitter model and the proposed two-state transmitter model. In Section III we develop the family of coherent and noncoherent two-state detectors. In Section IV we study the performance of the proposed detectors and give simulation results in Section V.

II. Description of SOQPSK

A. CPM Signal Model

The SOQPSK signal in complex baseband representation is defined as a CPM [1]

$$s(t;\boldsymbol{\alpha}) \triangleq \sqrt{\frac{E_b}{T_b}} \exp\{j\psi(t;\boldsymbol{\alpha})\} \tag{1}$$

where E_b is the energy per bit and T_b is the bit duration. The transmitted symbol sequence is $\boldsymbol{\alpha} \triangleq \{\alpha_i\}$, where each symbol has a duration equal to T_b and is drawn from a *ternary* alphabet, i.e. $\alpha_i \in \{-1, 0, +1\}$. The phase of the signal, $\psi(t;\boldsymbol{\alpha})$, is a pulse train of the form

$$\psi(t;\boldsymbol{\alpha}) \triangleq 2\pi h \sum_i \alpha_i q(t - iT_b) \tag{2}$$

where $i \in \mathbb{Z}$ is the discrete-time index and $h = 1/2$ is the *modulation index*. The *phase pulse* $q(t)$ is defined as

$$q(t) \triangleq \begin{cases} 0 & t < 0 \\ \displaystyle\int_0^t f(\tau)\, d\tau & 0 \le t < LT_b \\ 1/2 & t \ge LT_b \end{cases} \tag{3}$$

where $f(t)$ is the *frequency pulse*, which has a duration of L bit times and an area of 1/2. When $L = 1$ the signal is *full-response* and when $L > 1$ it is *partial-response*. Due to the constraints on $f(t)$ and $q(t)$, and given the use of a rational modulation index, the phase in (2) may be expressed as

$$\psi(t;\boldsymbol{\alpha}) = \underbrace{2\pi h \sum_{i=n-L+1}^{n} \alpha_i q(t - iT_b)}_{\theta(t)} + \underbrace{\pi h \sum_{i=0}^{n-L} \alpha_i}_{\theta_{n-L}} \tag{4}$$

where $nT_b \le t < (n+1)T_b$. The *phase state* $\theta_{n-L} \in \{0, \pi/2, \pi, 3\pi/2\}$ can assume only four distinct values when taken modulo-2π, which gives $e^{j\theta_{n-L}} \in \{\pm 1, \pm j\}$.

In this paper, we focus on the two standardized versions of SOQPSK. The first, SOQPSK-MIL [15], is full-response with a rectangular-shaped frequency pulse

$$f_{\text{MIL}}(t) \triangleq \begin{cases} \frac{1}{2T_b}, & 0 \le t < T_b \\ 0, & \text{otherwise.} \end{cases} \tag{5}$$

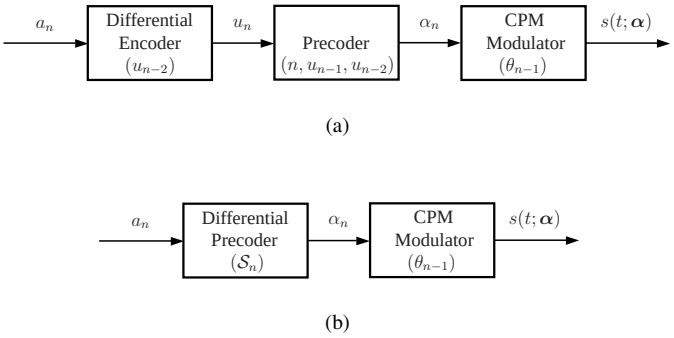

Fig. 1. Transmitter models for SOQPSK with (a) the original precoder with a four-state trellis and (b) the differential precoder with a two-state trellis.

The second, SOQPSK-TG [9], [16], is partial-response with $L = 8$ and a frequency pulse given by

$$f_{\text{TG}}(t) \triangleq A \frac{\cos\left(\frac{\pi\rho Bt}{2T_b}\right)}{1 - 4\left(\frac{\rho Bt}{2T_b}\right)^2} \times \frac{\sin\left(\frac{\pi Bt}{2T_b}\right)}{\frac{\pi Bt}{2T_b}} \times w(t) \tag{6}$$

where the window is

$$w(t) \triangleq \begin{cases} 1, & 0 \le \left|\frac{t}{2T_b}\right| < T_1 \\ \frac{1}{2} + \frac{1}{2}\cos\left(\frac{\pi}{T_2}\left(\frac{t}{2T_b} - T_1\right)\right), & T_1 \le \left|\frac{t}{2T_b}\right| \le T_1 + T_2 \\ 0, & T_1 + T_2 < \left|\frac{t}{2T_b}\right|. \end{cases}$$

The constant A is chosen such that the area of the pulse is equal to $1/2$ and $T_1 = 1.5$, $T_2 = 0.5$, $\rho = 0.7$ and $B = 1.25$.

B. Original SOQPSK Precoder and Four-State Trellis

With SOQPSK, the symbol sequence $\boldsymbol{\alpha}$, which is transmitted over the channel, is not the underlying information sequence; instead, the symbol sequence $\boldsymbol{\alpha}$ is derived from the original bit sequence $\boldsymbol{a} \triangleq \{a_i\}$ by the series of operations shown in Fig. 1 (a). The first of these operations is a *double differential encoder* [17] given by

$$u_n = a_n \oplus u_{n-2}, \qquad a_n, u_n \in \{0, 1\} \tag{7}$$

where $\oplus$ is the modulo-2 addition operator with identity 0. The differential encoding rule in (7) can be summarized as "change phase on 1" since an input of $a_n = 1$ causes the output value u_n to change relative to the state value u_{n-2}. The state memory of the differential encoder (u_{n-2}) is explicitly labled in Fig. 1 (a).

The second operation in Fig. 1 (a) is the *SOQPSK precoder*, which converts the differentially encoded sequence $\boldsymbol{u} \triangleq \{u_i\}$ into a ternary data sequence $\boldsymbol{\alpha}$, with elements $\alpha_n \in \{-1, 0, +1\}$, according to the rule [18]

$$\alpha_n(\boldsymbol{u}) = (-1)^{n+1}(2u_{n-1} - 1)(u_n - u_{n-2}). \tag{8}$$

For convenience, we drop the cumbersome notation $\alpha_n(\boldsymbol{u})$ in favor of the more streamlined notation α_n, but we emphasize the fact that α_n is a function of the input u_n and three binary-valued state variables: n-even/n-odd, u_{n-1}, and u_{n-2}. The state memory of the precoder is explicitly labeled in Fig. 1 (a).

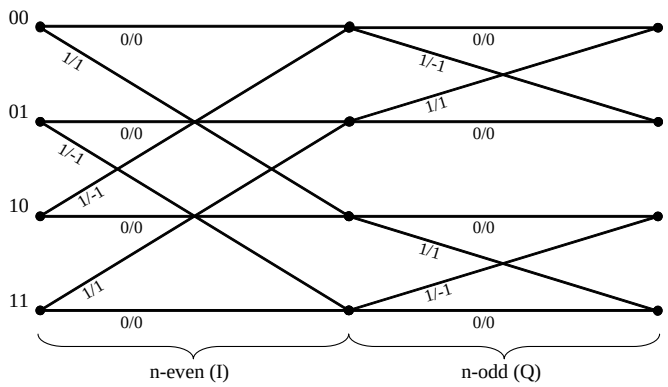

Fig. 2. Four-state time-varying trellis for the original precoder. The states are labeled with the state vector S_n and the branches are labeled with the input-bit/output-symbol pair a_n/α_n.

The precoder imposes three important constraints on the ternary data [18]:

1) While α_n is viewed as being *ternary*, in any given bit interval α_n is actually drawn from one of two *binary* alphabets, $\{0, +1\}$ or $\{0, -1\}$.
2) When $\alpha_n = 0$, the binary alphabet for α_{n+1} switches from the one used for α_n, when $\alpha_n \neq 0$ the binary alphabet for α_{n+1} does not change; this rule can be summarized as "switch alphabets on $\alpha_n = 0$."
3) A value of $\alpha_n = +1$ cannot be followed by $\alpha_{n+1} = -1$, and vice versa (this is implied by the previous constraint).

The last operation in Fig. 1 (a) is a conventional CPM modulator with $h = 1/2$ and the desired pulse shape $f_{\text{MIL}}(t)$ or $f_{\text{TG}}(t)$. For the special case of full-response CPM ($L = 1$), the only state variable within the CPM modulator is the phase state θ_{n-1}, which is explicitly labeled in Fig. 1 (a). In Section III we show how partial-response SOQPSK-TG can be modeled as a full-response CPM at the receiver; thus, the full-response model is the only case that must be considered as it can be applied to both versions of SOQPSK.

Fig. 2 shows the four-state time-varying trellis that describes the SOQPSK precoder in Fig. 1 (a) [8]. In this trellis, n-even/n-odd is not treated as a state variable (since this would require an 8-state trellis) but is handled instead with the time-varying sections of the trellis. The remaining precoder state variables are u_{n-1} and u_{n-2}. For convenience, we combine these variables to form $S_n \in \{00, 01, 10, 11\}$; these are ordered (u_{n-2}, u_{n-1}) for n-even and (u_{n-1}, u_{n-2}) for n-odd [18]. This means that the inphase (I) bit of the pair is always most significant and the quadrature (Q) bit of the pair is always least significant. The states in Fig. 2 are labeled with S_n and the branches are labeled with the input-bit/output-symbol pair a_n/α_n.

The advantage of the four-state precoder trellis is that its state variable S_n has a *one-to-one correspondence* with the phase state θ_{n-1} of the full-response CPM modulator that follows the precoder. In other words, a separate trellis is not required by the CPM modulator, and the entire system in Fig. 1 (a) is described by the four-state time-varying trellis in Fig. 2. The mapping from precoder trellis states to CPM phase states is [8]

$$\begin{aligned} 00 &\leftrightarrow \frac{3\pi}{2}, \qquad 01 \leftrightarrow \pi, \\ 10 &\leftrightarrow 0, \qquad 11 \leftrightarrow \frac{\pi}{2}. \end{aligned} \tag{9}$$

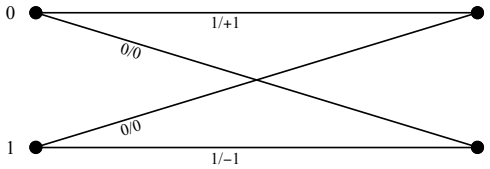

Fig. 3. Two-state trellis for the differential precoder. The states are labeled with the state vector $\mathcal{S}_n$ and the branches are labeled with the input-bit/output-symbol pair a_n/α_n.

C. Modified SOQPSK Precoder and Two-State Trellis

The SOQPSK precoder in (8) can be *combined* with the differential encoder in (7) to produce a *differential precoder*. The steps are given in the Appendix and the resulting expression is

$$\alpha_n = (-1)^{\mathcal{S}_n} a_n, \qquad a_n, S_n \in \{0, 1\}, \tag{10}$$

where the *sign state* $\mathcal{S}_n$ is updated with the operation

$$\mathcal{S}_{n+1} = (\mathcal{S}_n + \alpha_n + 1) \bmod 2 \tag{11a}$$

or equivalently

$$\mathcal{S}_{n+1} = (\mathcal{S}_n + a_n + 1) \bmod 2. \tag{11b}$$

This simplified series of transmitter operations is shown in block diagram form in Fig. 1 (b). We point out that the binary-valued sign state $\mathcal{S}_n$ is the only state variable required by the differential precoder, as explicitly labeled in Fig. 1 (b).

All of the binary-to-ternary constraints are clearly visible in (10) and (11a); since the input bit a_n is drawn from a binary alphabet, α_n is also drawn from a binary alphabet whose "sign" is controlled by the sign state $\mathcal{S}_n$; the switching rule for the binary alphabets is "switch alphabets on $\alpha_n = 0$," which is exactly how (11a) works. Furthermore, an elegant side effect of the differential precoder is that it makes the binary-to-ternary mapping "systematic" in the sense that one can easily identify the information bits in the ternary symbol sequence: $a_n = 0$ always maps to $\alpha_n = 0$ and $a_n = 1$ always maps to $\alpha_n = \pm 1$. This also means that the "change phase on 1" rule is directly observable in the output of the differential precoder since $\alpha_n = \pm 1$ changes the phase of the CPM signal.

Fig. 3 shows the two-state *time-invariant* trellis that describes the differential SOQPSK precoder in Fig. 1 (b) and equations (10) and (11). The states in Fig. 3 are labeled with $\mathcal{S}_n$ and the branches are labeled with the input-bit/output-symbol pair a_n/α_n.

The obvious advantage of the two-state trellis is its simplicity with respect to the four-state time-varying trellis in Fig. 2. Unfortunately, the two-state simplification does not do

anything to reduce the number of CPM phase states θ_{n-1}. Thus, a four-state trellis is still required to fully (i.e. optimally) describe the entire system in Fig. 1 (b). In the next section we will show how a simple *decision feedback* scheme can be employed at the detector to resolve the value of the phase state θ_{n-1}; this technique allows the simple two-state trellis to be successfully applied to SOQPSK and yields asymptotically optimal performance.

III. Decision Feedback SOQPSK Detectors

A. Received Signal Model

The received signal is modeled as

$$r(t) = s(t;\boldsymbol{\alpha})e^{j\phi(t)} + n(t) \tag{12}$$

where $n(t)$ is complex-valued additive white Gaussian noise (AWGN) with single-sided power spectral density N_0 and $\phi(t)$ is the carrier/channel phase which, for the moment, we assume to be perfectly known and zero-valued. (i.e. coherent detection). Since the transmitted signal $s(t;\boldsymbol{\alpha})$ has memory, the optimal detector must perform maximum likelihood sequence detection (MLSD). This is efficiently implemented via the Viterbi algorithm (VA), which is summarized below. In what follows, we refer to estimated and hypothesized values of a quantity w as $\hat{w}$ and $\tilde{w}$ respectively. Also, $\hat{w}$ and $\tilde{w}$ can assume the same values as w itself.

The VA operates on a trellis diagram, such as the one in Fig. 2. Over the duration of a symbol interval, the transmitted signal is in one of its possible states, S_n, the exact value of which is unknown to the receiver. Given the received signal, the likelihood that the transmitter is in a particular hypothetical state $\tilde{S}_n$ at time step n is quantified by the *cumulative metric* $\lambda_n(\tilde{S}_n)$. A cumulative metric is maintained for each state in the trellis. These metrics are updated by extending each branch from its starting state $\tilde{S}_n$ to its ending state $\tilde{E}_n$ via the recursion

$$\lambda_{n+1}(\tilde{E}_n) = \lambda_n(\tilde{S}_n) + \mathrm{Re}\left\{z(n,[\tilde{a}_n,\tilde{S}_n])\right\} \tag{13}$$

where $\mathrm{Re}\{\cdot\}$ is the real part of a complex number and $z(n,[\tilde{a}_n,\tilde{S}_n])$ is a generic *branch metric increment*, which is a function of the starting state $\tilde{S}_n$ and the branch symbol $\tilde{a}_n$; we refer to $[\tilde{a}_n,\tilde{S}_n]$ as the *branch vector*. In the case of SOQPSK, there are two branches that merge into each ending state $\tilde{E}_n$. The merging branch with the maximum metric is declared the *survivor* and its metric is stored for later use in the next round of updates.

This general VA framework will be used for both the four-state and two-state SOQPSK detectors. In order to realize such simple detectors for SOQPSK-TG, we must first summarize how partial-response SOQPSK-TG is handled at the receiver as if it were a full-response signaling scheme.

B. Branch Metric Increment Using Pulse Truncation

One technique for reducing the complexity of SOQPSK-TG at the receiver is known as pulse truncation (PT) [12], [13]. This approach stems from the fact that frequency pulses which are long and smooth are oftentimes near-zero for a significant portion of their duration. This is the case for $f_{\mathrm{TG}}(t)$ in (6). Using these arguments, we base the detector on a frequency pulse which has been truncated to a duration of one bit/symbol time (full-response). Of course, the detector uses a *phase* pulse instead of a *frequency* pulse, so we translate these arguments accordingly and obtain a modified phase pulse

$$q_{\mathrm{PT}}(t) = \begin{cases} 0, & t < 0 \\ q(t+(L-1)T_b/2), & 0 \le t \le T_b \\ 1/2, & t > T_b. \end{cases} \tag{14}$$

Note that the phase pulse in (14) is defined for all values of t; however, its time-varying portion has been shortened by a total of $(L-1)T_b$ and is restricted to the interval $[0,T_b]$. The truncation is centered such that half is applied to the beginning of the pulse and half to the end. Since $q_{\mathrm{PT}}(t)$ has variations only in the time interval $[0,T_b]$ it behaves like a full-response pulse.

The truncated pulse can be used in a standard CPM-type branch metric increment [1]

$$\begin{aligned} z_{\mathrm{PT}}(n,[\tilde{a}_n,\tilde{S}_n]) \triangleq e^{-j\tilde{\theta}_{n-1}} \int_{nT_b}^{(n+1)T_b} & r(t+(L-1)T_b/2) \\ & \times e^{-j2\pi h\tilde{\alpha}_n q_{\mathrm{PT}}(t-nT_b)}dt. \end{aligned} \tag{15}$$

The hypothesized branch vector $[\tilde{a}_n,\tilde{S}_n]$ has a one-to-one correspondence with a hypothesized ternary symbol $\tilde{\alpha}_n$ and a hypothesized CPM phase state $\tilde{\theta}_{n-1}$, as shown in Fig. 2 and Eq. (9), respectively. There are three complex-valued filter outputs needed to implement (15) (one for each possible value of the ternary $\tilde{\alpha}_n$).

While the notation in (14) and (15) is valid for SOQPSK-MIL and SOQPSK-TG, in the case of SOQPSK-MIL ($L=1$) the pulse $q_{\mathrm{MIL}}(t)$ is already full-response and no truncation takes place; thus the filters needed to implement (15) are *matched filters* (MFs). For this reason, we refer to (15) as the "MF metric" in the case of SOQPSK-MIL since it is in fact the *optimal* CPM-type metric. In the case of SOQPSK-TG, we refer to (15) as the "PT metric" and it results in *near-optimal* performance, as discussed in Sections IV and V.

C. Branch Metric Increment Using the PAM Representation

The PAM representation of CPM [10], [11] is a well-known technique where the right-hand side of (1) can be written as

$$s(t;\boldsymbol{\alpha}) = \sqrt{\frac{E_b}{T_b}} \sum_{k=0}^{R-1} \sum_{i} b_{k,i} g_k(t - iT_b) \tag{16}$$

which is simply a linear combination of R pulses $g_k(t)$ that are modulated by *pseudo-symbols* $b_{k,i}$. The pseudo-symbols are derived from the original data symbols α_i by a nonlinear mapping. The full definitions needed to describe the pulses and pseudo-symbols for SOQPSK are somewhat lengthy and do not contribute in a meaningful way to the present discussion; these definitions are found in [11].

TABLE I

THE RELATIONSHIP BETWEEN THE TERNARY BRANCH SYMBOL α_n, AND THE PSEUDO-SYMBOLS $\beta_k(\alpha_n)$ FOR SOQPSK.

α_n	$\beta_0(\alpha_n)$	$\beta_1(\alpha_n)$
-1	$\exp\{-j\pi/2\} = -j$	$\exp\{-j\pi/4\} = \frac{\sqrt{2}}{2}(1-j)$
0	1	$\cos(\pi/4) = \frac{\sqrt{2}}{2}$
$+1$	$\exp\{+j\pi/2\} = +j$	$\exp\{+j\pi/4\} = \frac{\sqrt{2}}{2}(1+j)$

For the present case of SOQPSK, an important property of the PAM technique is the following: when (16) is approximated with the first two terms in the outer summation, i.e.

$$s(t;\boldsymbol{\alpha}) \approx \sqrt{\frac{E_b}{T_b}} \sum_{k=0}^{1} \sum_{i} b_{k,i} g_k(t - iT_b) \tag{17}$$

the pseudo-symbols that remain, $b_{0,i}$ and $b_{1,i}$, can be described by the full-response trellis in Fig. 2. Thus, the PAM approximation in (17) can be used to realize four-state detectors for partial-response SOQPSK (and SOQPSK-TG in particular).

Using (17), the PAM-based branch metric increment is given by [8]

$$z_{\text{PAM}}(n, [\tilde{a}_n, \tilde{S}_n]) = e^{-j\tilde{\theta}_{n-1}} \sum_{k=0}^{1} y_k(n) [\beta_k(\tilde{\alpha}_n)]^* \tag{18}$$

where $(\cdot)^*$ is the complex conjugate. The pseudo-symbols $\beta_k(\cdot)$, $0 \le k \le 1$, in (18) are listed in Table I. The sampled matched MF output is

$$y_k(n) = \int_{nT_b}^{(n+L+1-k)T_b} r(t) g_k(t - nT_b)\, dt, \qquad 0 \le k \le 1, \tag{19}$$

where the PAM pulses $g_k(t)$ serve as the impulse responses of the MFs. The hypothesized branch vector $[\tilde{a}_n, \tilde{S}_n]$ has a one-to-one correspondence with $\tilde{\alpha}_n$ and $\tilde{\theta}_{n-1}$, as discussed before. In this case, each possible value of $\tilde{\alpha}_n$ corresponds to a row in Table I. The PAM pulses $g_0(t)$ and $g_1(t)$ are shown in [8, Fig. 6] for SOQPSK-TG.

Here again, the notation in (18) and (19) is valid for SOQPSK-MIL and SOQPSK-TG. In the case of SOQPSK-MIL, the exact PAM representation has only $R = 2$ terms so the approximation in (17) turns out to be exact. Thus, (18) is *optimal* in the case of SOQPSK-MIL. In the case of SOQPSK-TG, the exact PAM representation has $R = 4374$ terms, so (17) is truly an approximation and (18) results in a *near-optimal* detector, as discussed in Section IV and V.

D. Noncoherent Branch Metric Increment

Up to this point, we have considered the case where the carrier/channel phase is perfectly known and is zero; this case corresponds to coherent detection. A closely related case is when $\phi(t)$ is perfectly known but is non-zero; this case also corresponds to coherent detection and it requires that the generic VA increment in (13) be augmented to become $e^{-j\phi(t)} z(n, [\tilde{a}_n, \tilde{S}_n])$, where $z(n, [\tilde{a}_n, \tilde{S}_n])$ is again a generic placeholder for any of the branch metric increments defined above.

When $\phi(t)$ is unknown but slowly varying so that it is roughly constant over several bit times, then we have the case that has received much attention over the years for differential and noncoherent detection, e.g. [19], [20]. Using the noncoherent approach in [20] as a starting point, and the modified version of this approach proposed in [21], we obtain a noncoherent formulation $z_{\text{NC}}(n, [\tilde{a}_n, \tilde{S}_n])$ of the generic branch metric increment as

$$z_{\text{NC}}(n, [\tilde{a}_n, \tilde{S}_n]) = Q_n^*(\tilde{S}_n) z(n, [\tilde{a}_n, \tilde{S}_n]) \tag{20}$$

where the *phase reference* $Q_n(\cdot)$ is defined via the recursion

$$Q_{n+1}(\tilde{E}_n) = aQ_n(\tilde{S}_n) + (1-a) z(n, [\tilde{a}_n, \tilde{S}_n]) \tag{21}$$

where $0 < a < 1$ is the *forgetting factor* and its choice trades performance for constant phase offset versus robustness against phase variations. The noncoherent metric increment $z_{\text{NC}}(n, [\tilde{a}_n, \tilde{S}_n])$ is used in the VA exactly as specified by the placeholder in (13). The order of operations between (13) and (21) is important. The cumulative metric update (13) is performed first, which determines the survivors at each ending state. The phase reference update (21) is performed afterward for each ending state, $\tilde{E}_n$, using $Q_n(\tilde{S}_n)$ and $z(n, [\tilde{a}_n, \tilde{S}_n])$ from the surviving branch at each ending state, i.e *per-survivor processing* (PSP) [22].

E. Two-State Detectors for SOQPSK

As mentioned earlier, the difficulty with the two state trellis in Fig. 3 is that a one-to-one correspondence between the sign state $\mathcal{S}_n$ and the CPM phase state θ_{n-1} does not exist. Thus, when given the branch vector for the *two-state* trellis, $[\tilde{a}_n, \tilde{\mathcal{S}}_n]$, there is not enough information to compute the branch metric updates in (15) and (18). We propose decision feedback as a means of overcoming this problem.

As stated earlier, at the end of each symbol interval, a surviving branch is declared at each ending state $\tilde{E}_n$ in the trellis. We use $\hat{\alpha}_n(\tilde{E}_n)$ to denote the symbol associated with the surviving branch at each ending state $\tilde{E}_n$. In the decision-feedback VA, a *cumulative phase* $\hat{\theta}_{n-1}(\tilde{S}_n)$ is maintained for each state $\tilde{S}_n$ in the trellis, in addition to the above-mentioned cumulative metric $\lambda_n(\tilde{S}_n)$. Once the survivors have been declared, the cumulative phase for each ending state is updated via the recursion

$$\hat{\theta}_n(\tilde{E}_n) = \left[\hat{\theta}_{n-1}(\tilde{S}_n) + \pi h \hat{\alpha}_n(\tilde{E}_n)\right] \mod 2\pi. \tag{22}$$

As it turns out, in the case of the four-state detector the cumulative phase $\hat{\theta}_{n-1}(\tilde{S}_n)$ is identical to the phase state $\tilde{\theta}_{n-1}$ provided the four cumulative phases are initialized according to (9) at the start of the algorithm. This is equivalent to saying that, given the proper initialization, the two branches merging at each ending state in the four-state trellis will result in the same value for the cumulative phase. This is true by definition of the phase state in (4) and the cumulative phase in (22). Thus, the decision feedback does not introduce any sub-optimality to the four-state detectors.

In the case of the two-state detector, using $\hat{\theta}_{n-1}(\tilde{\mathcal{S}}_n)$ instead of $\tilde{\theta}_{n-1}$ does make the detector suboptimal, but it is a necessary step in order to implement the detector in the first place. The impact of decision feedback on the performance of the two-state detectors is now studied.

IV. Performance Analysis

The bit-error probability of SOQPSK with coherent detection in AWGN is described using error events and minimum distance concepts. The normalized squared Euclidean distance of CPM is [1]

$$d^2 = \frac{\log_2 M_{\text{info}}}{2T_b} \int |s(t;\boldsymbol{\alpha}_{\text{Tx}}) - s(t;\boldsymbol{\alpha}_{\text{Rx}})|^2 dt \qquad (23)$$

where $\log_2 M_{\text{info}}$ is the number of bits per symbol (for SOQPSK we have $M_{\text{info}} = 2$).

A. Minimum Distance Error Event

The minimum distance error event for the four-state SOQPSK detectors occurs when the transmitted and received *bit* sequences satisfy

$$\begin{aligned} \boldsymbol{a}_{\text{Tx}} &= \cdots, a_{e-1}, a_e, a_{e+1}, a_{e+2}, a_{e+3}, \cdots \\ \boldsymbol{a}_{\text{Rx}} &= \cdots, a_{e-1}, \overline{a}_e, a_{e+1}, \overline{a}_{e+2}, a_{e+3}, \cdots \end{aligned} \qquad (24)$$

In words, this is a double *bit* error event where the first bit error occurs at some arbitrary bit location a_e and the second bit error occurs with bit a_{e+2}. In [8] it was shown that when $a_{e+1} = 0$, the precoded *symbol* sequences satisfy $\pm\boldsymbol{\gamma}_0$, where

$$\boldsymbol{\gamma}_0 = \boldsymbol{\alpha}_{\text{Tx}} - \boldsymbol{\alpha}_{\text{Rx}} = \cdots, 0, -1, 0, +1, 0, \cdots \qquad (25)$$

and a squared distance of d_0^2 results. It was also shown in [8] that when $a_{e+1} = 1$, the precoded symbol sequences satisfy $\pm\boldsymbol{\gamma}_1$, where

$$\boldsymbol{\gamma}_1 = \boldsymbol{\alpha}_{\text{Tx}} - \boldsymbol{\alpha}_{\text{Rx}} = \cdots, 0, +1, +2, +1, 0, \cdots \qquad (26)$$

and a squared distance of d_1^2 results. These cases are easily verified by examining the four-state trellis in Fig. 2.

B. Additional Error Event for Two-State Detectors

For the two-state detectors, an additional error event is introduced and occurs when the transmitted and received *bit* sequences satisfy

$$\begin{aligned} \boldsymbol{a}_{\text{Tx}} &= \cdots, a_{e-1}, a_e, a_{e+1}, a_{e+2}, \cdots \\ \boldsymbol{a}_{\text{Rx}} &= \cdots, a_{e-1}, \overline{a}_e, \overline{a}_{e+1}, a_{e+2}, \cdots \end{aligned} \qquad (27)$$

In words, this is a double *bit* error event where the first bit error occurs at some arbitrary bit location a_e and the second bit error occurs with the following bit a_{e+1}. In this case, it is easily verified from Fig. 2 that the precoded symbol sequences satisfy $\pm\boldsymbol{\gamma}_2$, where

$$\boldsymbol{\gamma}_2 = \boldsymbol{\alpha}_{\text{Tx}} - \boldsymbol{\alpha}_{\text{Rx}} = \cdots, 0, +1, +1, 0, \cdots \qquad (28)$$

We denote the squared distance in this case by d_2^2.

TABLE II
Range of distance values in the set $\{d_{2,l}^2\}$ for the two-state SOQPSK detectors.

Configuration		$\min_l \left\{d_{2,l}^2\right\}$	$\max_l \left\{d_{2,l}^2\right\}$
MIL-MF	($d_0^2 = 1.73$)	2.00	2.00
MIL-PAM	($d_0^2 = 1.73$)	2.83	3.03
TG-PT	($d_0^2 = 1.60$)	1.71	2.23
TG-PAM	($d_0^2 = 1.60$)	2.57	3.35

C. Probability of Bit Error

The PT and PAM approximations discussed earlier result in *mismatched detectors* [12], [13], i.e. the detector is no longer matched to the transmitted signal. The mismatched detectors require the analysis to be more intricate. The minimum distance error event is still given by (24), and the two-state detectors still have the additional error event (27), but instead of having a single distance value in each case, say d_0^2, we get a *set* of distance values, $\{d_{0,l}^2\}$. For example, with SOQPSK-TG the optimal (fully matched) detector has $d_0^2 = 1.60$. When the four-state PT detector is used, the distance is slightly influenced by the values of the bits surrounding the error event on each side, $\{a_{e-k}\}_{k=1}^{3}$ and $\{a_{e+k}\}_{k=3}^{5}$, due to the partial-response phase pulse that is present in the transmitted signal. This results in a set of distance values $\{d_{0,l}^2\}_{l=0}^{63}$ that are clustered around the value $d_0^2 = 1.60$ and range in value from 1.38 to 1.77. The methods for calculating these distances are discussed in [12], [13], [23]

Taking this behavior into account, the final expression for the union bound on the bit-error probability of the four-state detectors is

$$P_{b,4} \le \frac{1}{|d_{0,l}|} \sum_{\{d_{0,l}^2\}} Q\left(\sqrt{d_{0,l}^2 \frac{E_b}{N_0}}\right) + \frac{1}{|d_{1,l}|} \sum_{\{d_{1,l}^2\}} Q\left(\sqrt{d_{1,l}^2 \frac{E_b}{N_0}}\right) \qquad (29)$$

where E_b/N_0 is the bit energy to noise ratio, $|\cdot|$ denotes the cardinality (number of elements) of a given set, and

$$Q(x) = \frac{1}{\sqrt{2\pi}} \int_x^\infty e^{-u^2/2} du. \qquad (30)$$

For example, with the MF detector for SOQPSK-MIL, we have singleton sets of $d_0^2 = 1.73$ and $d_1^2 = 2.36$, so (29) simplifies to a summation of only two terms. In the case of SOQPSK-TG, (29) contains the 128 terms in $\{d_{0,l}^2\}_{l=0}^{63}$ and $\{d_{1,l}^2\}_{l=0}^{63}$ that are clustered around the values $d_0^2 = 1.60$ and $d_1^2 = 2.59$.

For the two-state detectors, the union bound on the bit-error probability is the same as that of the four-state detectors but with an additional summation, i.e.

$$P_{b,2} \le P_{b,4} + \frac{1}{|d_{2,l}|} \sum_{\{d_{2,l}^2\}} Q\left(\sqrt{d_{2,l}^2 \frac{E_b}{N_0}}\right). \qquad (31)$$

Since (29) and (31) differ only by the terms introduced by the additional error event in (27), the values in $\{d_{2,l}^2\}$, which

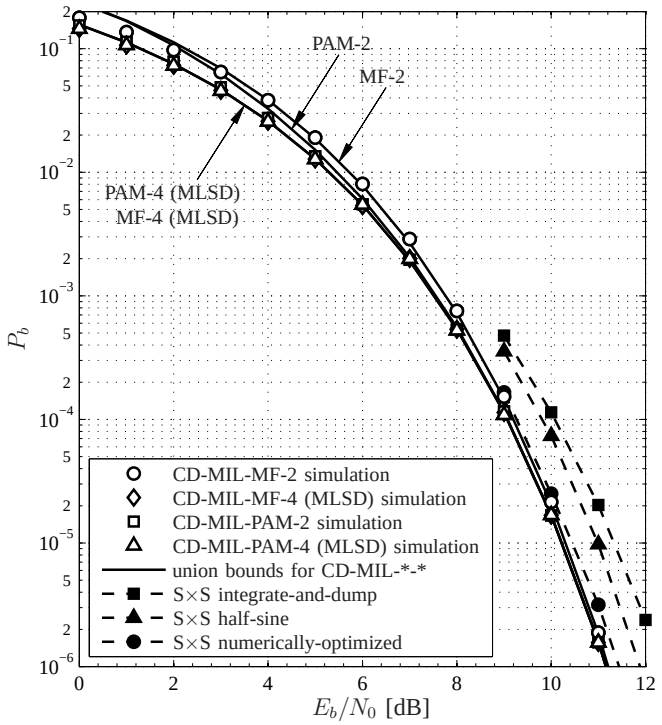

Fig. 4. Performance of reduced-complexity coherent detectors for SOQPSK-MIL.

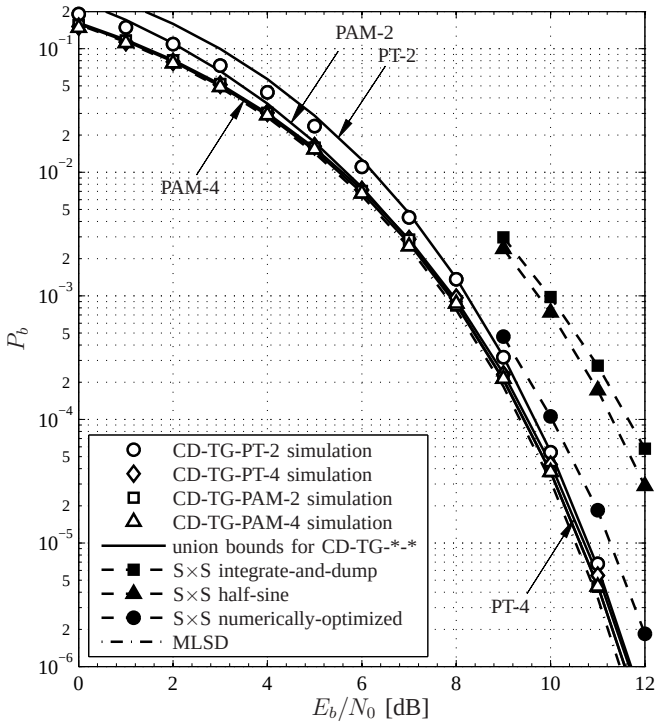

Fig. 5. Performance of reduced-complexity coherent detectors for SOQPSK-TG.

are summarized in Table II, are the key to quantifying the performance of the two-state detectors relative to the four-state detectors. The first observation from Table II is that, with all four of the two-state configurations, the distances in $\{d_{2,l}^2\}$ *exceed* the value of d_0^2, i.e. the minimum distance is *not worsened* by the two-state detectors. This means that the two-state detectors each have a performance that is asymptotically equivalent (i.e. for large E_b/N_0) to their four-state counterpart. The second observation from Table II is that the PAM-based detectors have values in $\{d_{2,l}^2\}$ that are far greater than d_0^2, while the MF and PT detectors have values that are relatively close to d_0^2; thus, even for low to moderate ranges of E_b/N_0 we would expect the PAM-based detectors to have performance identical to the four-state detectors, while the MF and PT detectors should have minor losses for low to moderate values of E_b/N_0. These expectations are borne out in the simulation results we present next.

V. Simulation Results

There are two carrier/channel conditions (coherent and noncoherent), two modulation types (SOQPSK-MIL and SOQPSK-TG), two branch metric types (MF/PT and PAM), and two trellis sizes (two-state and four-state) that have been discussed above. This yields a total of sixteen detector configurations, eight of which involve a newly proposed two-state decision-feedback detector. The primary intent of the simulation results herein is to confirm that the two-state detectors have negligible or minor performance losses compared to their four-state counterparts. In the figures that follow, we use a notation with four fields, "channel-modulation-metric-trellis," to refer to each of the sixteen cases, i.e. "ND-MIL-PAM-2" refers to noncoherent detection of SOQPSK-MIL using PAM-based branch metrics and the two-state trellis.

We first examine the case of coherent detection. Fig. 4 shows performance curves for the four SOQPSK-MIL configurations (i.e. "CD-MIL-*-*," where "*" indicates all cases in a given field are considered). In the low E_b/N_0 region of the figure, the two-state union bounds given by (31) are not necessarily tight with respect to the simulation points (shown as *points only*, with *no connections* between points); however, the union bounds and the simulation points show close agreement rapidly as E_b/N_0 increases, which verifies the accuracy of the performance analysis above. Furthermore, the results anticipated in the previous section are confirmed. The simulation points for the two-state PAM-based detector indicate no observable degradation with respect to the four-state MLSD detectors (across the entire simulation range of E_b/N_0), while the simulation points for the two-state MF-based detector indicate a slight performance degradation for small E_b/N_0 that narrows and approaches zero at the large end of the simulated E_b/N_0 range. For comparative purposes, we also show simulation curves for symbol-by-symbol ("S×S") detection for the larger values of E_b/N_0 for three cases of the internal symbol-by-symbol detection filter: integrate-and-dump, half-sine, and numerically optimized (from [3]). Regardless of the internal detection filter, the symbol-by-symbol detectors all perform worse than the trellis-based detectors.

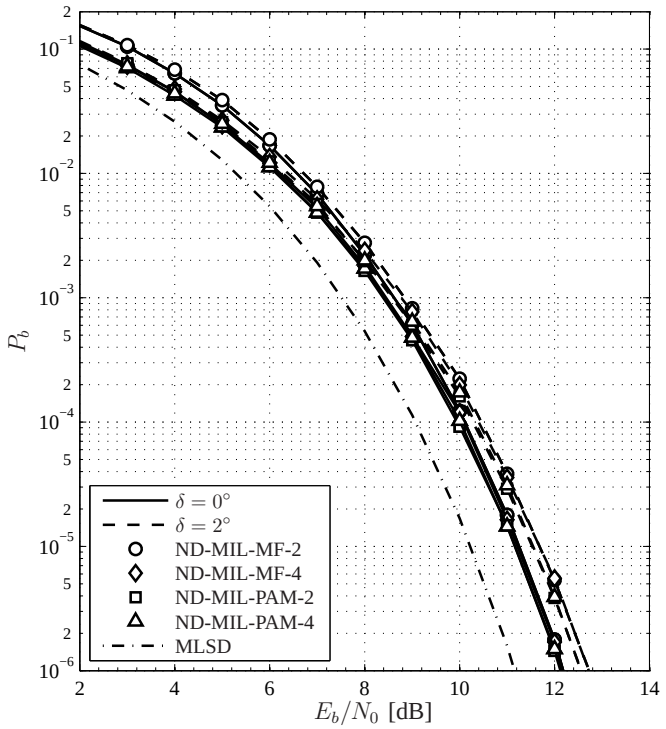

Fig. 6. Performance of reduced-complexity noncoherent detectors for SOQPSK-MIL.

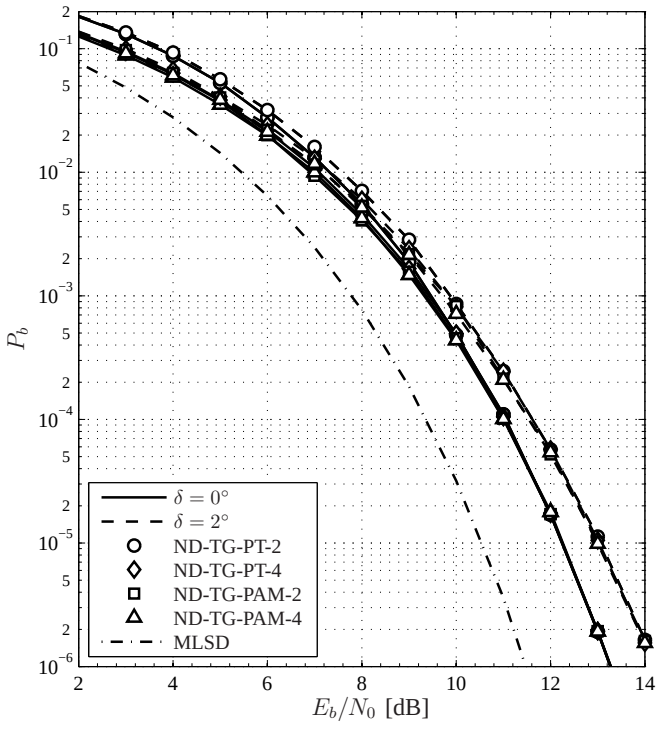

Fig. 7. Performance of reduced-complexity noncoherent detectors for SOQPSK-TG.

Fig. 5 shows performance curves for the four coherent SOQPSK-TG configurations (CD-TG-*-*). As with the previous figure, the two-state union bounds and the simulation points show close agreement rapidly as E_b/N_0 increases. Also, the two-state PAM-based detector shows no observable degradation with respect to the four-state PAM detector, while the two-state PT-based detector has a slight performance degradation with respect to the four-state PT-based detector. We give a reference curve for the 512-state MLSD scheme since it is not simulated due to its impracticality. Regardless of the trellis size, the PAM technique has a 0.1 dB inherent advantage over the PT technique, as originally reported in [8]. Here also we show three comparison cases of the symbol-by-symbol detector, which illustrate the more-pronounced performance gains that are realized with trellis-based detection of SOQPSK-TG.

We now turn to the case of noncoherent detection. Here we drop the comparison with symbol-by-symbol detection, and we also drop the comparison between analytical and simulation results since the analysis was performed only for coherent detection. However, we are now interested in the performance of the various detectors over a phase noise channel; we use a common model for such a channel where the time-varying carrier/channel phase is of the form [24]

$$\phi(t) = \phi(t - T_b) + \nu_n, \qquad nT_b \le t < (n+1)T_b \qquad (32)$$

where $\{\nu_n\}$ is a sequence of independent and identically distributed Gaussian random variables with zero mean and variance δ^2. Fig. 6 shows simulation results for noncoherent detection of SOQPSK-MIL (ND-MIL-*-*) with $\delta = 0°/\text{symbol}$ (i.e. AWGN only) and $\delta = 2°/\text{symbol}$, which is a total of eight curves; in all cases, the value[1] of the forgetting factor is $a = 0.875$. The simulation curves in Fig. 6 quickly separate into groups with a common value of δ, and within these groups the four detectors are ranked the same performance-wise as they are in coherent detection. The fact that the two-state detectors have essentially identical performance to their four-state counterparts (except for the PT case at low E_b/N_0) over the various channel conditions is significant since it demonstrates that the savings in complexity do not come at the expense of bit error performance. Fig. 7 shows that last set of simulation results, which are for noncoherent detection of SOQPSK-TG (ND-TG-*-*) with $\delta = 0°/\text{symbol}$ (i.e. AWGN only) and $\delta = 2°/\text{symbol}$, where the results also fall into the pattern established above.

VI. Conclusion

We have successfully developed a family of two-state decision-feedback detectors for SOQPSK-MIL and SOQPSK-TG using pulse amplitude modulation (PAM) and pulse truncation (PT) techniques; separate coherent and noncoherent formulations of these detectors were given. Using performance

[1]Although the values chosen for δ and a are typical with those in other studies, we do not attach special significance to these values since our intent is mainly to compare the performance of the noncoherent two-state detectors with the noncoherent four-state detectors and not to design for any particular channel conditions.

analysis, we have shown that these two-state detectors each have performance that is asymptotically equivalent to their four-state counterparts. This is a satisfying result due to the minimal two-state level of complexity achieved by these detectors. These simple detection schemes are applicable in settings where high-performance and low complexity are needed to meet restrictions on power consumption and cost.

APPENDIX

We show how the differential precoder in (10) and (11) is obtained by combining the differential encoder in (7) with the SOQPSK precoder in (8).

We begin by stating some conversions between Boolean variables and binary antipodal variables. A generic Boolean variable $w_n \in \{0,1\}$ can be converted into an antipodal variable $w'_n \in \{\pm 1\}$ by

$$w'_n = 2w_n - 1 \tag{33}$$

or

$$-w'_n = (-1)^{w_n}. \tag{34}$$

Also, the differential encoder in (7) and the SOQPSK precoder in (8) can be expressed in terms of antipodal bits as

$$u'_n = (-a'_n) \cdot u'_{n-2}, \qquad a'_n, u'_n \in \{\pm 1\} \tag{35}$$

and

$$\alpha_n = \frac{1}{2}(-1)^{n+1} u'_{n-1}(u'_n - u'_{n-2}), \tag{36}$$

respectively; as before, the "change phase on 1" rule is in effect for the differential encoder. We obtain an intermediate result by substituting (35) into (36), which yields

$$\begin{aligned}
\alpha_n &= \frac{1}{2}(-1)^{n+1} u'_{n-1}(\underbrace{u'_n}_{-a'_n u'_{n-2}} - u'_{n-2}) \\
&= (-1)^{n+1} \underbrace{\frac{-a'_n - 1}{2}}_{-a_n} u'_{n-1} u'_{n-2} \\
&= (-1)^n a_n u'_{n-1} u'_{n-2}
\end{aligned} \tag{37}$$

where (33) is also applied.

Next, we show how (37) simplifies to (10). Substituting (35) with itself recursively gives

$$\begin{aligned}
u'_{n-1} u'_{n-2} &= \prod_{i=0}^{n-1} (-a'_i) \\
&= \prod_{i=0}^{n-1} (-1)^{a_i} \\
&= (-1)^{\sum_{i=0}^{n-1} a_i}
\end{aligned} \tag{38}$$

where (34) is also applied. Inserting (38) into (37) results in

$$\begin{aligned}
\alpha_n &= (-1)^{n+\sum_{i=0}^{n-1} a_i} a_n \\
&= (-1)^{\mathcal{S}_n} a_n
\end{aligned}$$

where the sign state $\mathcal{S}_n$ is defined by either of the recursions in (11). These recursions are equivalent because the rule "switch alphabets on $a_n = 0$" is the same as "switch alphabets on $\alpha_n = 0$" in the case of the differential encoder.

REFERENCES

[1] J. B. Anderson, T. Aulin, and C.-E. Sundberg, *Digital Phase Modulation*. New York: Plenum Press, 1986.

[2] M. J. Dapper and T. J. Hill, "SBPSK: A robust bandwidth-efficient modulation for hard-limited channels," in *Proc. IEEE Military Commun. Conf.*, Oct. 1984.

[3] M. Geoghegan, "Optimal linear detection of SOQPSK," in *Proc. Int. Telemetering Conf.*, Oct. 2002.

[4] L. Li and M. Simon, "Performance of coded OQPSK and MIL-STD SOQPSK with iterative decoding," *IEEE Trans. Commun.*, vol. 52, pp. 1890–1900, Nov. 2004.

[5] M. Simon and T.-Y. Yan, "Cross-Correlated Trellis-Coded Quadrature Modulation." U.S. patent filed Oct. 1999.

[6] M. Simon and T.-Y. Yan, (1999, May), "Performance evaluation and interpretation of unfiltered Feher-patented quadrature phase-shift keying (FQPSK)," *Telecommun. and Mission Operations Prog. Rep.*, vol. [Online]. Available: http://tmo.jpl.nasa.gov/tmo/progress_report/42-137/137C.pdf.

[7] M. Simon and T.-Y. Yan, "Unfiltering Feher-patented quadrature phase-shift keying (FQPSK): Another interpretation and further enhancements: Parts 1, 2," *Appl. Microwave Wireless Mag.*, vol. 12, pp. 76–96/100–105, Feb./Mar. 2000.

[8] E. Perrins and M. Rice, "Reduced-complexity approach to iterative detection of SOQPSK," *IEEE Trans. Commun.*, vol. 55, pp. 1354–1362, Jul. 2007.

[9] Range Commanders Council Telemetry Group, Range Commanders Council, White Sands Missile Range, New Mexico, *IRIG Standard 106-04: Telemetry Standards*, 2004. (Available on-line at http://www.ntia.doc.gov/osmhome/106.pdf).

[10] P. A. Laurent, "Exact and approximate construction of digital phase modulations by superposition of amplitude modulated pulses (AMP)," *IEEE Trans. Commun.*, vol. 34, pp. 150–160, Feb. 1986.

[11] E. Perrins and M. Rice, "PAM representation of ternary CPM," to be published in *IEEE Trans. Commun.*

[12] T. Aulin, C.-E. Sundberg, and A. Svensson, "Viterbi detectors with reduced complexity for partial response continuous phase modulation," in *Proc. National Telecommun. Conf., NTC'81*, (New Orleans, LA), pp. A7.6.1–A7.6.7, Nov./Dec. 1981.

[13] A. Svensson, C.-E. Sundberg, and T. Aulin, "A class of reduced-complexity Viterbi detectors for partial response continuous phase modulation," *IEEE Trans. Commun.*, vol. 32, pp. 1079–1087, Oct. 1984.

[14] S. Lin and D. Costello, *Error Control Coding*. New York: Prentice Hall, 2004.

[15] D. I. S. Agency, "Department of Defense interface standard, interoperability standard for single-access 5-kHz and 25-kHz UHF satellite communications channels." Tech. Rep. MIL-STD-188-181B, Department of Defense, Mar. 1999.

[16] T. Hill, "A non-proprietary, constant envelope, variant of shaped offset QPSK (SOQPSK) for improved spectral containment and detection efficiency," in *Proc. IEEE Military Commun. Conf.*, Oct. 2000.

[17] M. K. Simon, "Multiple-bit differential detection of offset QPSK," *IEEE Trans. Commun.*, vol. 51, pp. 1004–1011, Jun. 2003.

[18] M. Simon, *Bandwidth-Efficient Digital Modulation With Application to Deep-Space Communication*. New York: Wiley, 2003.

[19] D. Divsalar and M. K. Simon, "Multiple-symbol differential detection of MPSK," *IEEE Trans. Commun.*, vol. 38, pp. 300–308, Mar. 1990.

[20] G. Colavolpe and R. Raheli, "Noncoherent sequence detection," *IEEE Trans. Commun.*, vol. 47, pp. 1376–1385, Sep. 1999.

[21] R. Schober and W. H. Gerstacker, "Metric for noncoherent sequence estimation," *Electron. Lett.*, vol. 35, pp. 2178–2179, Dec. 1999.

[22] R. Raheli, A. Polydoros, and C.-K. Tzou, "Per-survivor processing: A general approach to MLSE in uncertain environments," *IEEE Trans. Commun.*, vol. 43, pp. 354–364, Feb./Apr. 1995.

[23] E. Perrins and M. Rice, "Reduced complexity detectors for multi-h CPM in aeronautical telemetry," *IEEE Trans. Aerosp. Electron. Syst.*, vol. 13, pp. 286–300, Jan. 2007.

[24] A. Demir, A. Mehrotra, and J. Roychowdhury, "Phase noise in oscillators: A unifying theory and numerical methods for characterization," *IEEE Trans. Circuits Syst.*, vol. 47, pp. 655–674, May 2000.